IEEE Access
Multidisciplinary ⋮ Rapid Review ⋮ Open Access Journal

Received 25 June 2023, accepted 27 July 2023, date of publication 7 August 2023, date of current version 25 August 2023.

Digital Object Identifier 10.1109/ACCESS.2023.3302916

RESEARCH ARTICLE

Performance Evaluation of 3.3 kV SiC MOSFET and Schottky Diode Based Reverse Voltage Blocking Switch for Medium Voltage Current Source Inverter Application

SNEHA NARASIMHAN[1], (Graduate Student Member, IEEE), AJIT KANALE[2], (Member, IEEE), SUBHASHISH BHATTACHARYA[1], (Fellow, IEEE), AND JAYANT B. BALIGA[1], (Life Fellow, IEEE)

[1]Department of Electrical and Computer Engineering, North Carolina State University, Raleigh, NC 27695, USA
[2]Wolfspeed Inc., Durham, NC 27709, USA

Corresponding author: Sneha Narasimhan (snarasi7@ncsu.edu)

ABSTRACT SiC power devices are used for medium-voltage (MV) motor drive and traction applications due to their higher temperature operation, switching frequencies, and higher efficiencies than Si-based devices. This article investigates three 3.3 kV reverse blocking or current switch configurations for their suitability in MV current-source inverter (CSI) applications. The three configurations are 1) Type I - SiC MOSFET and series Schottky diode; 2) Type II - SiC MOSFETs connected in common-source (CS); and 3) Type III - SiC MOSFETs connected in common-drain (CD) configuration. The switch configurations are characterized by comparing their on-state and switching performance at different junction temperatures varying from 25°C to 125°C. The results are used to evaluate three-phase CSI losses with three different switch configurations and choose the preferred switch configuration for MV-based CSI applications based on inverter efficiency while considering a wide range of operating points. The permissible limits of a 3.3 kV Type I switch-based CSI are presented, thus providing a safe operating area (SOA) of the switch configuration for a CSI application. Finally, the CSI is built using Type I switch configuration and is experimentally validated with an R-L load.

INDEX TERMS 3.3 kV SiC diode, 3.3 kV SiC MOSFET, common-source (CS), common-drain (CD), current source inverter (CSI), current switch, medium-voltage (MV), reverse-voltage blocking (RVB) switch, wide-bandgap devices, GaN, SiC.

I. INTRODUCTION

Silicon Carbide (SiC) power devices are being adopted for motor drives, solid-state transformers, and traction applications due to their high breakdown voltage ratings, superior thermal conductivity, low on-state voltage, and high-frequency operation compared to Si-based power devices. The successful development of commercial SiC power devices in the medium voltage (MV) range (2.3 kV - 15 kV) has led to a renewed interest in adopting them in utility and traction applications [1], [2]. Adopting 3.3 kV SiC MOSFETs and Schottky diodes to replace Si IGBTs in modules has been demonstrated to reduce switching losses by half and improve the power density [3]. 6.5 kV Schottky-barrier diode (SBD) embedded SiC MOSFETs have been packaged in modules to achieve high-power density inverter systems [4]. 10 kV SiC MOSFETs have been paralleled to achieve high-current levels and demonstrated in megawatt-class solid-state transformer application [5], facilitating a 75% reduction in weight and a 50% reduction in size compared to conventional transformers.

Following the invention of the Si IGBT, MV applications have overwhelmingly preferred voltage-source inverter (VSI) topologies over thyristor-based current-source inverters (CSIs) [6]. CSI topologies have an inherent short-circuit withstand capability, single-stage boost conversion, and

The associate editor coordinating the review of this manuscript and approving it for publication was Qinfen Lu.

This work is licensed under a Creative Commons Attribution-NonCommercial-NoDerivatives 4.0 License.
For more information, see https://creativecommons.org/licenses/by-nc-nd/4.0/

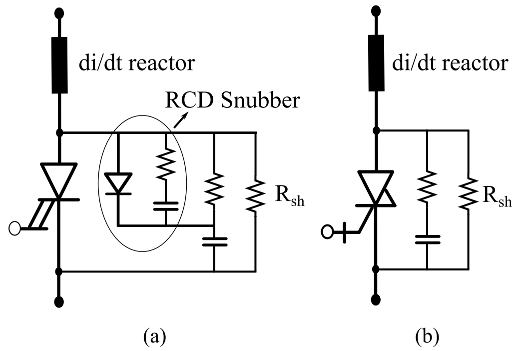

FIGURE 1. Switch configuration for existing CSI drives in MV applications - a) GTO-based switch leg with RCD snubber, RC snubber, sharing resistor (R_{sh}) and di/dt reactor, and b) SGCT based switch leg RC snubber, R_{sh} and di/dt reactor [14].

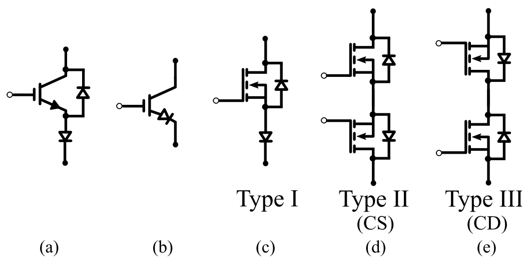

FIGURE 2. Switch configurations without di/dt reactor for CSI drives in MV applications - a) Reverse-blocking IGBT, b) IGBT with an anti-parallel diode and a series diode, c) Type I switch with a MOSFET and a series diode, d) Type II switch with a common-source (CS) configuration, and e) Type III switch with a common-diode (CD) configuration.

higher temperature operation of the coupling inductor compared to the dc-bus capacitors used in VSI topology [7], which favor their adoption for aerospace and transportation applications [8]. The advent of high-voltage rated WBG devices promises high-frequency and high-temperature operating capability, thus enabling exploration of CSIs [9], [10]. The relative lack of research articles on SiC-based reverse voltage blocking (RVB) switches also necessitates studies to qualify these emerging devices for various MV applications.

Hybrid reverse-blocking and bidirectional switch topologies have been investigated for CSI-based high-speed machine applications using 900 V - 1200 V rated SiC MOSFETs and Schottky diodes [11]. A novel test-bed has been proposed for characterization and model extraction of 3.3 kV current switches under hard-switching and soft-switching conditions [12] to be used for soft-switching based solid-state transformer. A 10 kV current switch is characterized in [13]; however, a comparison of the three different configurations of the current switch is not discussed. In [9], the losses are compared for a high-speed machine (HSM)-based CSI and VSI system using 3.3 kV SiC devices.

This paper discusses the static and dynamic characterization of three RVB switch configurations of MOSFET with series diode, MOSFETs connected in common-source (CS) or common-drain (CD) configuration assembled using 3.3 kV SiC MOSFETs and 3.3 kV SiC Schottky diodes. The device configurations are characterized for on-state behavior using

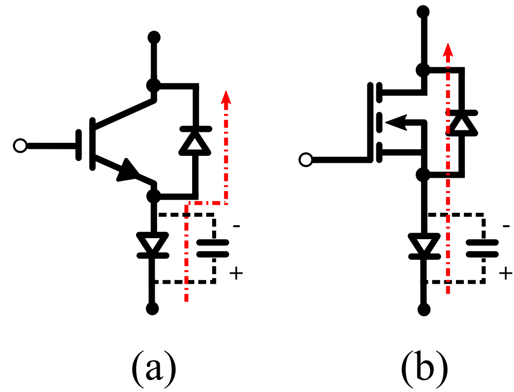

FIGURE 3. Diode reverse recovery current direction a) IGBT with an anti-parallel diode and a series diode, and b) MOSFET with a series diode.

a Keysight B1505A Curve Tracer [15] at 25°C and 175°C. The switching performance is evaluated at a dc-link current of 50 A at different voltages (−2500 V to 2500 V), junction temperatures (25°C, 125°C), and gate resistances ($R_g = 10\ \Omega$, 15 Ω, 20 Ω). Using the double pulse test (DPT) experiments, the measured loss data can be used to design a SiC MV-based CSI system and evaluate its switching frequency limits based on the safe operating area (SOA) of the RVB switch.

II. SWITCH CONFIGURATIONS

The existing MV-based CSIs use Gate Turn-off Thyristors (GTOs) and Symmetrical Gate Commutated Thyristors (SGCTs) as the RVB switch [16], [17]. To limit the di/dt of the switch, snubber circuits are used, as shown in Fig. 1. Also, the devices are connected in series to realize the voltage ratings, thereby requiring a series balancing resistor. The GTOs need a resistor, capacitor, and diode (RCD) snubber for over-voltage protection and limiting di/dt. With SGCTs, the RCD snubber can be eliminated, reducing the overall snubber's size. The SGCTs, however, still need the RC snubber. Additionally, the turn-on time and the tail currents of the SGCTs are lower than GTOs. The SGCTs also tend to operate at a higher switching frequency than the GTOs, thus slightly reducing the size of the passive components compared to GTO-based CSIs. However, the CSIs operate at a low switching frequency (200 Hz - 720 Hz) to improve the overall system efficiency, thereby increasing the passive components' size.

To realize RVB operation, the switch must block voltages in both directions and allow current flow in one direction. An IGBT with a diode in series acts as an RVB switch, as shown in Fig. 2(a). However, an anti-parallel diode is essential to accommodate reverse recovery losses of the series diode. Fig. 3(a) shows the reverse recovery current direction of the series diode during the turn-off of the diode while blocking negative voltage. Since the IGBT is a unidirectional current-carrying device, the anti-parallel diode helps to carry the reverse recovery current during the commutation of the current switches. Si PiN diodes employed for such purposes exhibit a tail current limiting the converter's switching fre-

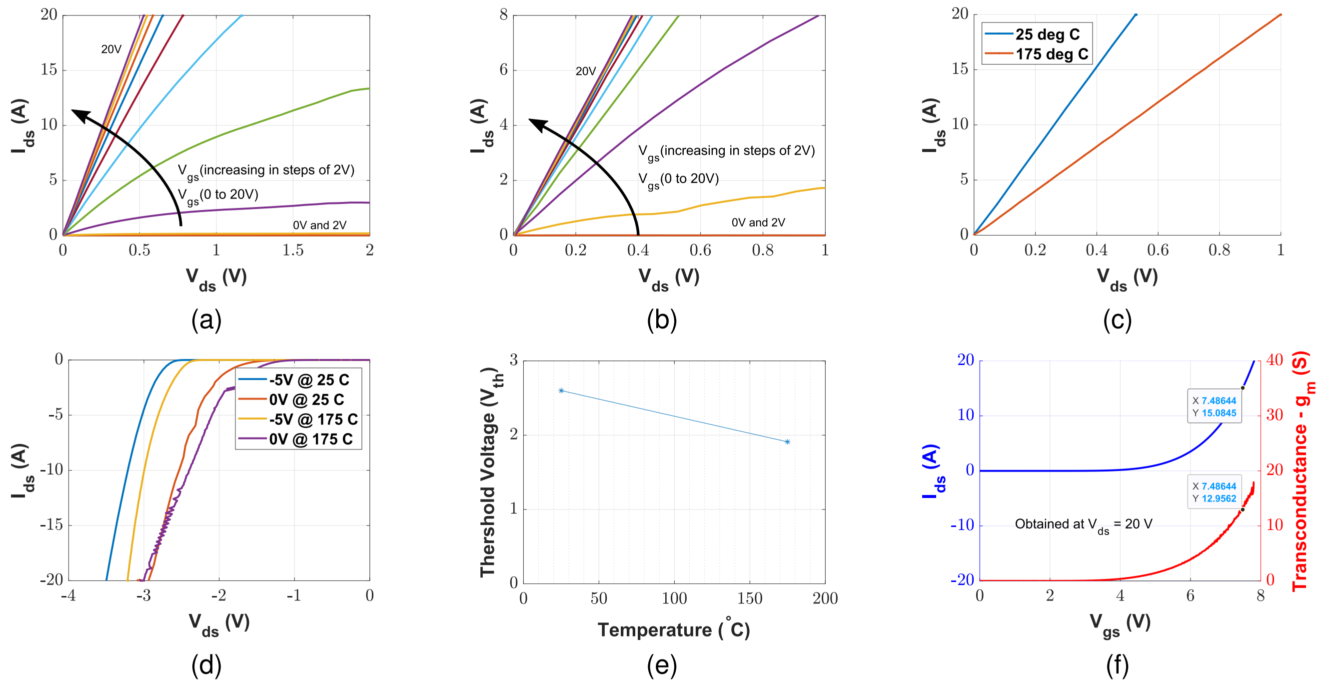

FIGURE 4. a) Output I-V MOSFET characteristic measured at room temperature, b) Output I-V MOSFET characteristic measured at 175°C, c) Output I-V characteristic at $V_{gs} = 20$ V and at room temperature and 175°C, d) Third quadrant characteristics of the MOSFET at $V_{gs} = 0$ V and $V_{gs} = -5$ V at room temperature and 175°C, e) Threshold voltage of the MOSFET measured at a drain current of 1 mA, and f) Transfer characteristics of the MOSFET measured at $V_{ds} = 20$ V and room temperature.

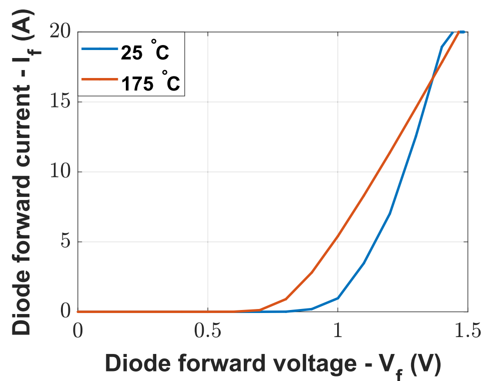

FIGURE 5. Output I-V diode characteristic measured at room temperature and at 175°C.

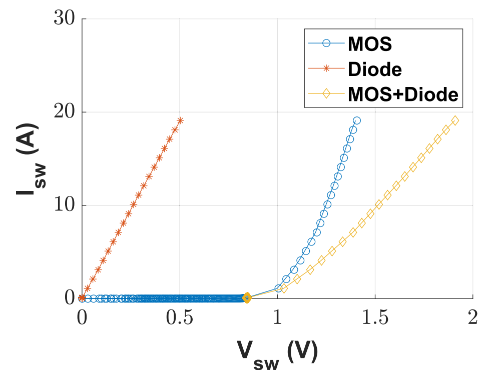

FIGURE 6. Combined output I-V characteristic at room temperature.

quency, resulting in the use of bulky passive components. The switching frequency limits of the IGBT-based current switch can be increased by replacing the Si PiN diode with the SiC Schottky diode [18]. However, this does not reduce the device count and results in an increased switch cost compared to the switches used for VSI applications. The increased conduction losses due to the series diode can be reduced with a Reverse Blocking IGBT (RB-IGBT), as shown in Fig. 2(b). The RB-IGBTs are commercially rated for 600 V and sampled for 1200 V and are preferred for soft-switching applications compared to hard-switching applications [19].

With SiC MOSFET-based RVB switches, the inherent body diode prevents the need for an anti-parallel diode, thus realizing the RVB switch using two devices. Fig. 3(b) shows the direction of the reverse recovery current through the series diode going through the MOSFET as it is a bidirectional device. To build an RVB switch, three configurations of switches are examined - Type I: a SiC MOSFET in series with a SiC Schottky diode; Type II: two back-to-back SiC MOSFETs with a common-source (CS) connection; and Type III: two back-to-back SiC MOSFETs with a common-drain (CD) connection. The different device configurations suitable to realize an RVB switch are shown in Fig. 2.

III. STATIC AND DYNAMIC CHARACTERIZATION

Static characterization of the 3.3 kV, 104 A, TO-247 4-lead SiC MOSFET (MSC025SMA330B4) and 3.3 kV, 90 A, TO-247 2-lead SiC Schottky diode (MSC090SDA330B2) was conducted using the Keysight B1505A curve tracer. The static characterization is performed at room temperature and

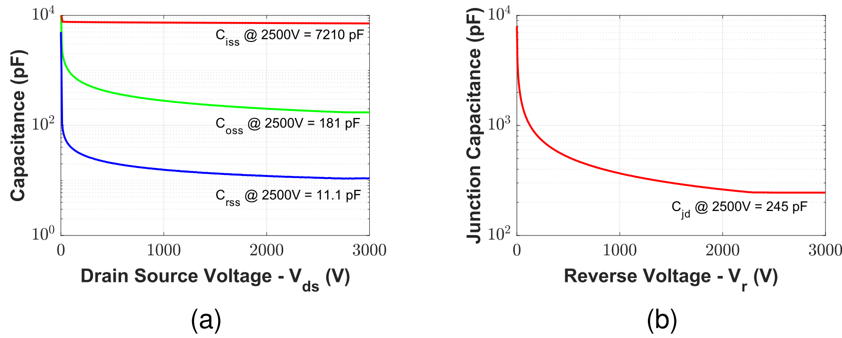

FIGURE 7. a) Variation of reverse transfer capacitance C_{rss}, input capacitance C_{iss}, and output capacitance C_{oss} with the voltage across the MOSFET b) Junction Capacitance of the diode.

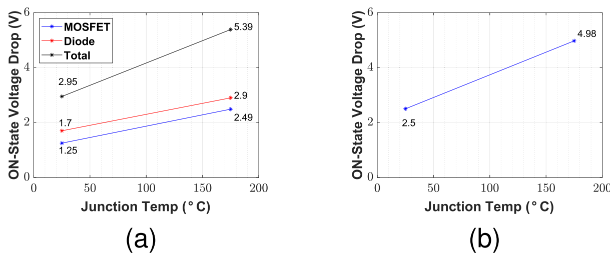

FIGURE 8. On-state voltage drop of a current switch at 50 A and variable junction temperatures with a) MOSFET and diode in series, and b) two MOSFETs in CS or CD configuration.

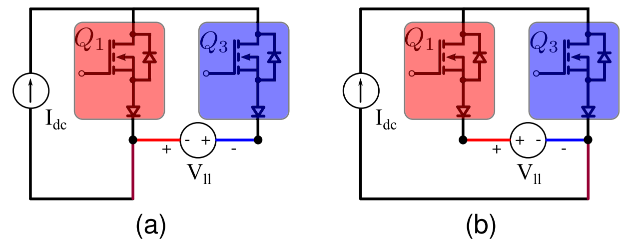

FIGURE 10. Commutation cells for a) Q_1 to Q_3 and losses of Q_3 is observed with $V_{ll} < 0$, and b) Q_3 to Q_1 and reverse recovery losses of Q_3 is observed with $V_{ll} > 0$.

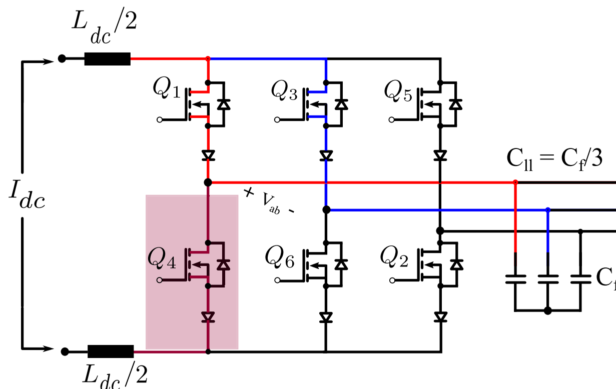

FIGURE 9. Three-phase current source inverter topology with Type I switches highlighting the current commutation of top switches Q_1 and Q_3 with Q_4 ON.

175°C. The dynamic characterization was conducted using the DPT circuit developed using the CSI commutation circuit at different case temperatures and gate resistance values.

A. STATIC CHARACTERIZATION

The first quadrant characteristics of the SiC MOSFET at 25°C and 175°C are shown in Fig. 4a and 4b, respectively. The on-state characteristics of the MOSFET are obtained at various gate voltages (V_{gs}) from 0 to 20 V. Fig. 4c shows the on-state characteristics of the MOSFET at 25°C and 175°C and at V_{gs} of 20 V. The MOSFET has an on-state resistance ($R_{ds,on}$) of 25 mΩ at a gate bias of 20 V at 25°C and an $R_{ds,on}$ of 48 mΩ at a gate bias of 20 V at 175°C. The increase in the on-state resistance with temperature is due to the positive temperature coefficient of the channel resistance, which is the most dominant component of SiC MOSFET on-resistance [20]. The third quadrant characteristics of the SiC MOSFET at 25°C and 175°C are shown in Fig. 4d. The reduction in the third quadrant voltage drop with increasing temperature can be attributed to the space charge physics of the P-i-N body diode [20].

The measured threshold voltage of the SiC MOSFET at a drain voltage (V_{ds}) of 0.1 V and a I_{ds} of 1 mA at 25°C and 175°C is shown in Fig. 4e. The decrease in threshold voltage with temperature can be attributed to increased intrinsic carrier concentration in the SiC MOSFET drift region [20]. The transfer characteristics of the SiC MOSFET measured with a drain bias of 20 V at 25°C is shown in Fig. 4f. The MOSFET has a transconductance of 13 S at a current (I_{ds}) of 15 A.

The first quadrant characteristics of the diode obtained at 25°C and at 175°C is shown in Fig. 5. When the MOSFET is connected in series with the diode, the IV characteristics of the current switch are the sum of the individual switch characteristics, as shown in Fig. 6. Additionally, the combined switch does not have a third-quadrant operation due to the presence of the series diode.

The measured input ($C_{iss} = C_{gs} + C_{gd}$), output ($C_{oss} = C_{ds} + C_{gd}$) and reverse transfer capacitances ($C_{rss} = C_{gd}$) of the SiC MOSFET are shown in Fig. 7a. The measurements are obtained at different blocking voltages at a 100 kHz frequency according to the JEDEC standards. The value of the junction capacitances is temperature invariant. The output capacitance contributes to the voltage over-shoot during turn-off caused by the current flowing through the drain-source

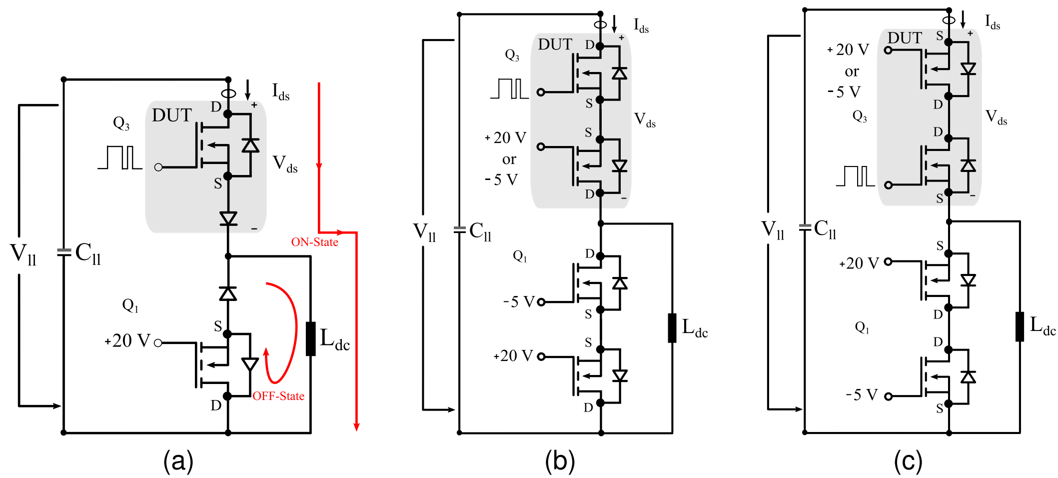

FIGURE 11. DPT Setup using a) Type I switch, b) Type II: Common-source (CS) switch, and c) Type III: Common-drain (CD) switch.

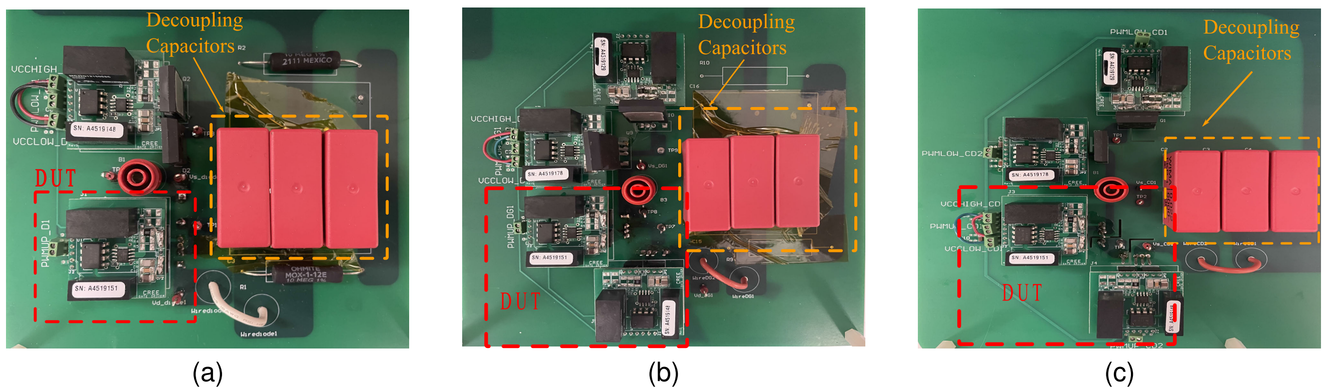

FIGURE 12. Hardware Setup using a) Type I switch, b) Type II (CS) switch, and c) Type III (CD) switch.

parasitic inductance in series with the output capacitance. The C_{rss}, also known as the Miller capacitance, mainly contributes to the shoot-through effect in switching modules. A smaller input capacitance results in faster slew rates of the drain currents and shorter switching delays [21]. The diode's junction capacitance is 245 pF at 2500 V, as shown in Fig. 7b.

For the Type I switch, the reverse recovery current of the series diode caused by the diode junction capacitance increases the turn-on switching loss. For Type II and Type III switches, the reverse recovery losses of the PiN body-diode of the MOSFET contribute to increased switching losses. To improve the third quadrant operation of the Type II or Type III switch, the reverse recovery losses of the PiN body diode can be reduced using a JBSFET, which has a JBS diode embedded with the MOSFET die to suppress the effect of the internal body diode [22].

B. ON-STATE VOLTAGE

The on-state voltage drop (V_{on}) of the current switch with a MOSFET and diode in series and the current switch with two MOSFET in series is shown in Fig. 8. The V_{on} is obtained at a I_{ds} of 50 A and different junction temperatures. The V_{on} of the individual MOSFET and diode is shown in Fig. 8a. The total conduction loss increases due to the presence of the diode. The CS and CD configurations achieve the lowest voltage drop when both MOSFET channels are used for current conduction. Hence, the series diode can be replaced with a MOSFET to reduce the conduction losses. Fig. 8b shows the on-state voltage drop with two MOSFETs in CS or CD configuration. The on-state voltage drop at 25°C for a Type I switch is 2.95 V, and the on-state voltage drop for a Type II and Type III switch is 2.5 V for a 50 A current. As the current increases, the on-state drop of the Type II and Type III switch significantly increases.

C. DYNAMIC CHARACTERIZATION

1) COMMUTATION OF THE CSI

Fig. 9 shows the three-phase CSI topology using Type I switches. L_{dc} is the dc-link inductor that generates the current source, and C_f is the line-neutral output filter capacitors. For a CSI, only one switch in the top leg and bottom leg can be ON at any instant. The commutation of the switches in the CSI occurs between Q_1, Q_3, Q_5 for the top leg and Q_4, Q_6, Q_2 for the bottom leg. Assuming that Q_4 is ON and the current commutates from Q_1 to Q_3 depending on the polarity of the voltage V_{ll}. Fig. 10 shows the equivalent commutation circuit

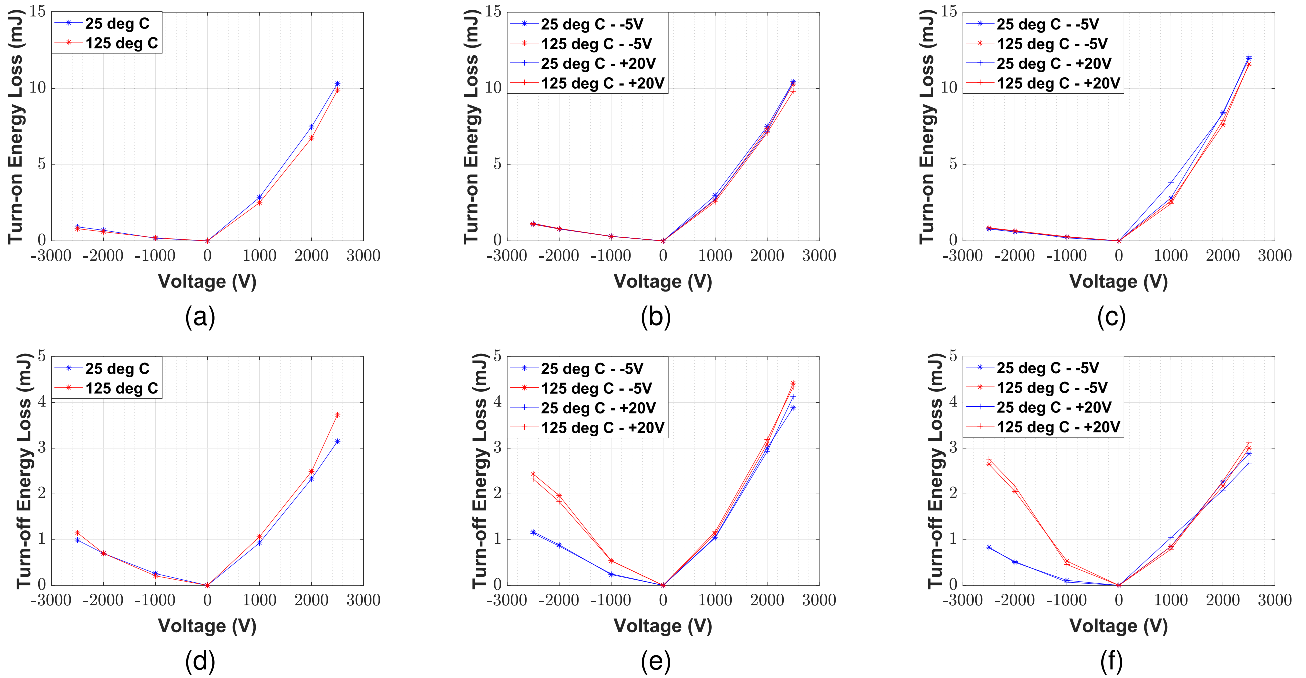

FIGURE 13. Losses are obtained for an external R_g of 20 Ω and I_{ds} of 50 A a) Turn-on losses of Type I switch, b) Turn-on losses of Type II (CS) switch, c) Turn-on losses of Type III (CD) switch, d) Turn-off losses of Type I switch, e) Turn-off losses of Type II (CS) switch, and f) Turn-off losses of Type III (CD) switch.

for $V_{ll} < 0$ (Fig. 10a), and $V_{ll} > 0$ (Fig. 10b). For $V_{ll} < 0$, when the current commutates from Q_1 to Q_3, the MOSFET in Q_3 is hard switched during turn-on, and the diode in Q_1 experiences reverse recovery losses. When the current commutates back from Q_3 to Q_1, the MOSFET in Q_3 experiences hard turn-off losses, and the diode in Q_1 experiences turn-on losses. This shows at any given instant, a single MOSFET and diode are involved in a commutation for a CSI, similar to that of a commutation in a VSI [23].

The commutation circuits are used to generate the DPT circuit, and details of the test circuit will be discussed in the next section. This analysis can also be extended for CSIs with CS or CD configurations.

2) TEST CIRCUIT

The DPT schematic for three configurations is shown in Fig. 11. The switches are kept in a common-source configuration for the DPT as generated with the commutation circuit shown in Fig. 10a. Since a current source is not readily available, the losses can be measured using a voltage source to generate the current. The top switch is the device under test (DUT) for all the configurations emulating the commutation of the current from Q_1 to Q_3. The device is turned on with a positive gate voltage (V_{gs}) of +20 V and turned off with a negative V_{gs} of −5 V. The gate pulses to the gate drive board are provided using a function generator. The lower switch is kept at +20V for the Type I switch, as shown in Fig. 11a. Fig. 11a shows the direction of the current when the DUT is turned ON and OFF. For the Type II and Type III switches, one of the switches in the DUT is pulsed while the other switch is kept at +20V or −5V and the losses of the DUT are measured. The lower switch of Type II and Type III switch is gated according to Fig. 11b and Fig. 11c.

An air-core 4 mH dc-link inductor helps to avoid the saturation of the core. The parasitic inductance is measured to be 8 pF at 100 MHz, which is negligible compared to the junction capacitance of the current switch. The inductor acts as the current source of the commutation circuit. The capacitor across the voltage source is a dc-capacitor of 120 uF and replicates the ac-side line-line filter capacitors. The delta-connected line-line capacitors are rated to $\frac{C_f}{3}$. Decoupling capacitors are placed close to the device to provide a low-impedance path for the high-frequency currents during the DUT switching. A Rogowski coil sensor CWTUM/06/B is used to measure the current through the device, and the voltage across the switch is measured using the high-voltage differential probe HVD 3605A. It is important to trim the device leads to minimize losses due to the lead inductance of the TO-247 package. To heat the device, the DUT is bent by 90 degrees, placed on the bottom of the board with a thermal pad, and heated using a hot plate. The thermal pad is placed on the drain of the MOSFET and cathode of the diode to provide isolation when heated using a hot plate.

The PCBs are being used for a 2.5 kV DC bus; it is important to maintain the creepage and clearance standard for PCB design at the voltage levels. The IPC-2221 standard is followed for selecting the spacings for the PCB [24], [25]. PCB keep-out layers are placed to achieve creepage isolation. Standard PCB material of FR-4 is used, and the thickness is determined based on its breakdown voltage of 150 to

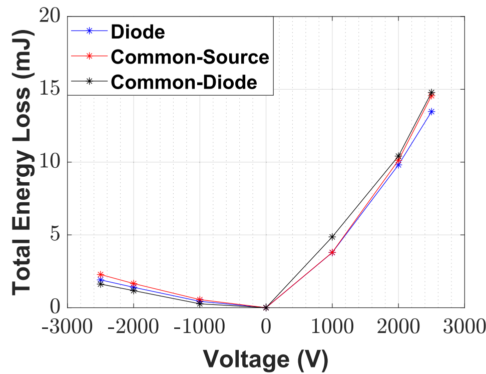

FIGURE 14. Total losses for Type I, Type II (CS), and Type III (CD) switches at 25°C, R_g of 20 Ω and I_{ds} of 50 A.

300 V/mil considering the effects of aging and manufacturing impurities [1]. However, the nominal breakdown voltage of FR-4 material is 800 V/mil which forms the basis for selecting the thickness of the PCB.

3) DPT RESULTS

The DPT is conducted at constant current and different voltage ratings. The current switch blocks voltage in both directions and allows current in one direction. V_{ds} varies from −2500 V to 2500 V, and I_{ds} is set to 50 A. The external turn-on and turn-off gate resistance (R_g) are set to 20 Ω. The turn-on losses of Type I, II, and III switches are shown in Fig. 13a, Fig. 13b and Fig. 13c. The turn-on and turn-off losses of Type I, II, and III switches are shown in Fig. 13d, Fig. 13e and Fig. 13f. The Type II and III switch losses are obtained when the series MOSFET of the DUT is provided a V_{gs} of −5 V or +20 V.

When a positive voltage is applied across the switch, the MOSFET exhibits hard turn-on and turn-off, thereby having higher losses. When a negative voltage is applied across the switch, all current switch types' turn-on loss is negligible in comparison to the turn-on losses at positive voltages. These losses are associated with the series diode or the non-switching MOSFETs in the DUT of the Type II or III configurations. Also, at negative voltages, the turn-off losses for the current switch are similar to the turn-on losses at the negative voltage at the room temperature of 25°C. These losses are associated with the reverse recovery losses of the series SiC diode for a Type I configuration or the PiN body diode for the Type II or Type III configurations. However, the turn-off losses for the Type II and Type III switches at 125°C increase by about 3.5 times that of the room-temperature value. This is associated with the increased reverse recovery losses of the PiN body diode with increased temperature [20].

Since the losses in the current switch are mainly observed during the turn-on transition, a zero-current-switching (ZCS) operation will reduce the total switching losses, improving system efficiency. Suppose a Type III switch is used for a zero-current switching (ZCS) operation, where the turn-on losses are reduced. In that case, the overall system loss decreases compared to a Type II switch operating at ZCS [26].

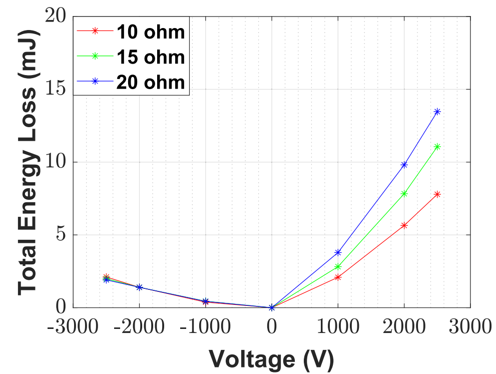

FIGURE 15. The total loss of the Type I switch at variable R_g of 20 Ω, 15 Ω, and 10 Ω at 25°C and I_{ds} of 50 A.

TABLE 1. The turn-on I_{pk} and turn-off di/dt and dV/dt at 2500V and 50A with R_g of 20 Ω at 25°C.

Switch Type	Turn-on	Turn-off	
	I_{pk} (A)	di/dt (A/ns)	dV/dt (V/ns)
Type I switch	75.04 A	-1.01	25.38
Type II (CS) switch	81.4 A	-1.41	25.23
Type III (CD) switch	82.68 A	-1	25.56

The turn-off losses increase with temperature, and the turn-on losses decrease with temperature due to the decrease in the threshold voltage at higher temperatures. However, the total switching losses increase by about 6% when the temperature changes from 25°C to 125°C at a V_{ds} of 2.5 kV DC bus and I_{ds} of 50 A for the Type I configuration. A similar trend is observed for the Type II and III configurations.

Fig. 14 shows the total loss of three different switch types at 25°C at an external R_g of 20 Ω. The variation in the total loss for three different configurations is about 10% at 2500 V. However, at −2500 V, it is about 18% between the three configurations and significantly lower than the losses obtained at positive voltages.

Fig. 15 shows the variation of the total loss of the Type I switch with different external R_g of 10 Ω, 15 Ω and 20 Ω at 50 A current. As the R_g increases, there is an increase in the total loss for positive voltages. This is because the turn-on and turn-off times increase with the increase in R_g, thereby increasing the turn-on and turn-off losses. However, the losses for negative voltages are similar for variation in the R_g and negligible compared to the losses during positive voltages primarily because these losses are contributed due to the series diode for the Type I switch. For the Type II and Type III switches, these losses are contributed due to the PiN body diode. The losses in the diodes are independent of the R_g values.

Fig. 16a shows the turn-off switching waveforms of the current switch in three different configurations at 2500 V and 50 A current when R_g is 20 Ω. Table. 1 shows the turn-on and turn-off di/dt and dV/dt. For the Type II switch, the lower dV/dt results in higher turn-off losses. The dV/dt of

TABLE 2. CSI System Parameters using 3.3 kV devices or 1.7 kV SiC devices.

Parameter	WBG CSI - 3.3 kV devices	WBG CSI - 1.7 kV devices
Rated output voltage	1.4 $kV_{ll,rms}$	690 $V_{ll,rms}$
Rated DC-current, I_{dc}	10 A or 50 A	20 A
Rated output power	15 kW or 80 kW	15 kW
Output power factor, $cos\ \Phi$	0.95	
Rated frequency, f	1000 Hz	
DC-link Inductor, L_{dc}	10 mH	20 mH
Output Filter Capacitor, C_f	1 uF or 5 uF	5 uF
Modulation scheme	SVPWM	
Gate voltage, V_{gs}	+20 V/-5 V	
Gate resistance, R_g	20 ohms	
Ambient Temperature, T_{amb}	50°C	

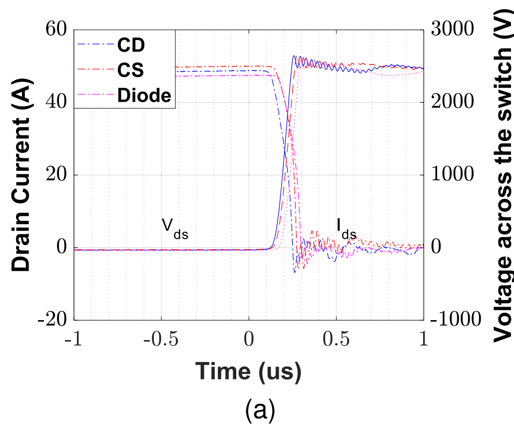

(a)

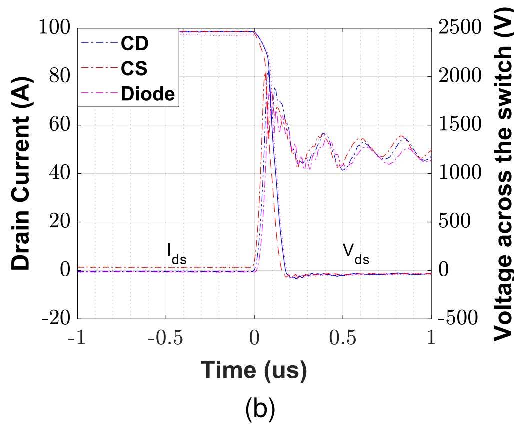

(b)

FIGURE 16. The turn-off losses (E_{off}) and the turn-on losses (E_{on}) at 2500 V, 50 A, 25°C and external gate resistance (R_g) of 20 Ω.

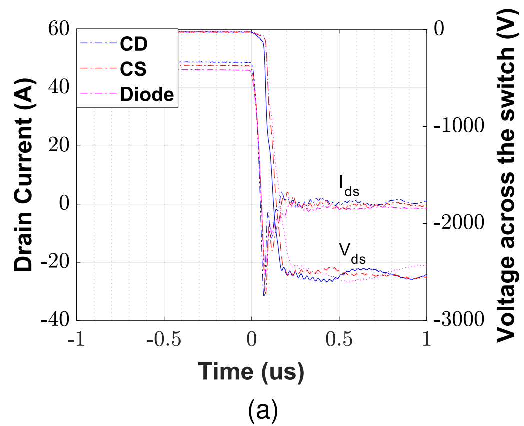

(a)

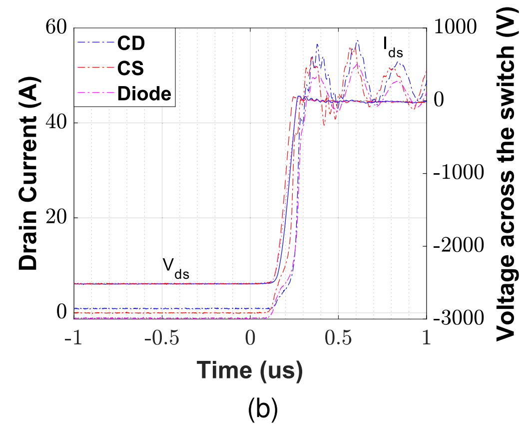

(b)

FIGURE 17. The turn-off losses (E_{off}) and the turn-on losses (E_{on}) at −2500 V, 50 A, 25°C and external gate resistance (R_g) of 20 Ω.

the remaining switch configurations decides the trend of the Type I and Type III switches, i.e., the losses of the Type I switch are greater than the Type III switch. Fig. 16b shows the turn-on switching waveforms of the current switch in three different configurations at 2500 V and 50 A current when the external R_g is 20 Ω. Based on the peak currents shown in Table. 1, the Type I switch has the lowest turn-on losses. For the Type I switch, during the positive voltage, the MOSFET acts as the forward voltage blocking switch, whereas during the negative voltage, the diode acts as the RVB switch. The reverse-recovery behavior of the diode is observed during turn-off at negative voltage, as shown in Fig. 17a. Fig. 17a shows the reverse recovery behavior of the diode due to the capacitive current during the turn-off transition. For the Type II (CS) and Type III (CD) switch, the reverse recovery behavior of the body diode of the MOSFET is shown during the negative transition. Fig. 17b shows the turn-on losses of the diode at negative voltage.

IV. DISCUSSION

A. REALIZING REVERSE BLOCKING SWITCH CONFIGURATIONS

Current switch implementations using SiC MOSFETs have a lower on-state voltage drop than those using Si IGBTs [27]. Additionally, Type II and Type III can achieve a lower

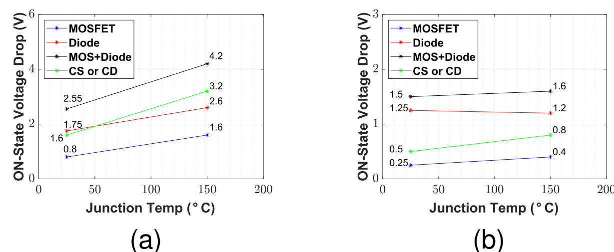

FIGURE 18. a) On-state voltage drop of a 1.7 kV current switch at 20 A current, and b) On-state voltage drop of a 3.3 kV current switch at 10 A current.

on-state voltage drop than the Type I switch configuration (see Fig. 2) due to the availability of two channels during current flow. The Type III switch-based three-phase converter design requires only five isolated gate driver power supplies compared to the Type II-based converter [28]. The Type II and Type III need two gate drivers per switch, increasing the system cost. The Type II-based system tends to have an easier gate-driver layout due to the CS configuration, and the Type III-based system tends to have easier fabrication due to the CD configuration.

It is worth mentioning that Type I switches can be fabricated on the same 4H-SiC wafer by placing the SiC MOSFET and diode chips adjacent to each other [29]. Simultaneous fabrication of heterogenous devices on the same wafer has been successfully demonstrated for 1.2 kV SiC devices [30]. The Type III (CD) switch configuration can also be implemented as a monolithic device [27] by fabricating two similarly rated SiC MOSFETs next to each other on the wafer and extracting the pair as a single semiconductor chip.

As mentioned above, the feasibility of monolithic chip realization for Type I and Type III switch configurations is conducive for large-scale manufacturing while also being scalable across device voltage ratings. 3.3 kV 4H-SiC reverse-blocking MOSFETs have been created [31] using complex fabrication techniques, including substrate removal, thin-wafer processing, and bottom-side ion-implantation precisely aligned to the MOSFET structure and edge-terminations on the top-side. Such complex fabrication techniques are not available in most manufacturing facilities. Thus, using discrete devices would be the way forward till the manufacturability of a single device is possible.

B. COMPARISON OF TYPE I AND CS OR CD SWITCH-BASED CSI

In [32], the author argues that bidirectional FETs are better for CSI applications. However, the best configuration will depend on the voltage and current ratings of the system. In this section, a comparison of the system losses of 15 kW rated systems using 1.7 kV devices with 20 A current, and 3.3 kV devices with 10 A current. Table. 2 shows the overall system parameters. The modulation scheme for the CSI is the space vector PWM (SVPWM). With Type II and Type III switches, it is important to provide dead-time and overlap-time to prevent dc-bus shoot through. The 4-step commutation method is used for the Type II and Type III based CSIs [33].

Table. 3 shows the conduction and switching loss at 20 A current using 1.7 kV devices and Table. 4 shows the conduction and switching loss at 10 A current using 3.3 kV devices. The switching losses of the system using 1.7 kV devices are lower primarily because of the lower blocking voltage than the switching losses of the system using 3.3 kV devices. The feature of lower switching losses can favor using 1.7 kV devices over 3.3 kV devices for similar power applications. Fig. 18 shows the on-state voltage drop of the 1.7 kV switches at 20 A current. For the Type I switch, the on-state voltage drop is significantly higher compared to Type II or Type III switches, thus increasing the conduction loss in a Type I-based system using 1.7 kV switches. Replacing the diode with the MOSFET reduces the conduction loss but increases the switching loss. The conduction loss decrease of 34 W compensates for the switching loss increase of 19 W, thus improving the overall system efficiency. Hence, a Type II or Type III-based switch configuration is preferred for a 20 A system using 1.7 kV devices.

Fig. 18b shows the on-state voltage drop of the 3.3 kV switches at 10 A current. The conduction losses are lower for the switch as the current conduction is lower than the 1.7 kV rated system. Also, this variation can arise due to the difference in parts. However, the switching losses significantly increase with increased voltage. Even though replacing the diode with the MOSFET provides a benefit in terms of conduction loss reduction of 16 W, the Type II or Type III configurations can't compensate for the increased switching loss of 56 W and thus don't provide any efficiency improvement. Hence, a Type I-based switch configuration is preferred for a 10 A system using 3.3 kV devices.

C. EVALUATION OF 3.3 kV BASED CSI

Table. 2 shows the overall system parameters using 3.3 kV devices and 50 A current. The conduction loss, switching loss, and total loss of a three-phase CSI system using 3.3 kV devices and 50 A current is shown in Table. 5. The ratio of the conduction loss of the diode to the MOSFET is 1.15 times. For a 10 A system, the ratio of the conduction loss of the diode to the MOSFET is 3.67 times. As the current increases, the conduction loss of the MOSFET becomes similar to the conduction loss of the diode. Thus, replacing the diode with the MOSFET reduces the conduction loss; however, it can't compensate for the increase in switching loss.

Fig. 19a shows the efficiency of the three switch types operating at variable operating temperatures. There is a 0.17% reduction in the efficiency at room temperature and a 0.25% reduction in efficiency at 125°C. Fig. 19b shows the efficiency of the three switch types operating at variable switching frequencies. There is a 0.17% reduction in the efficiency at 20 kHz switching frequency and a 0.63% reduction in efficiency at 60 kHz switching frequency. The efficiency of the CSI decreases with the increase in operating temperatures

TABLE 3. The switching loss, conduction loss, and total loss of a 3-phase CSI system for three switch types used using 1.7 kV devices in HSM application at a dc-link current of 20 A, 50°C ambient, and 20 kHz switching frequency.

System Loss at 20 A	Type I switch	Type II (CS) switch	Type III (CD) switch
Conduction Loss (W)	123 (M = 44 + D = 79)	89	89
Switching Loss (W)	13	32	34
Total Loss (W)	136	121	123
Efficiency (%)	99.1	99.2	99.2

TABLE 4. The switching loss, conduction loss, and total loss of a 3-phase CSI system for three switch types used using 3.3 kV devices in HSM application at a dc-link current of 10 A, 50°C ambient, and 20 kHz switching frequency.

System Loss at 10 A	Type I switch	Type II (CS) switch	Type III (CD) switch
Conduction Loss(W)	28 (M = 6 + D = 22)	12	12
Switching Loss (W)	61	108	117
Total Loss (W)	89	120	129
Efficiency (%)	99.5	99.3	99.2

TABLE 5. The switching loss, conduction loss, and total loss of a 3-phase CSI system for three switch types used using 3.3 kV devices in HSM application at a dc-link current of 50 A, 50°C ambient, and 20 kHz switching frequency.

System Loss at 50 A	Type I switch	Type II (CS) switch	Type III (CD) switch
Conduction Loss (W)	360 (M = 167 + D = 193)	327	345
Switching Loss (W)	175	332	334
Total Loss (W)	535	659	679
Efficiency (%)	99.4	99.2	99.2

across all configurations and follows a similar trend for the switching frequencies. Assuming an inverter efficiency of 99%, the Type I-based solution can operate at a switching frequency of 52 kHz, and the Type II and Type III-based CSI will result in an approximate switching frequency of 25 kHz. This will increase the size of the passives by about two times compared to the Type I solution. Thus, a Type I switch-based CSI system is preferred for 3.3 kV MV-based CSI across all operating temperatures and switching frequencies. To conclude, the Type I switch-based CSI system is the preferred solution for 3.3 kV device MV-based CSI.

For higher voltage systems ($\geq$3.3 kV), the conduction loss contribution of the MOSFET becomes similar to the diode, and hence replacing the diode with MOSFET does not provide any benefit [13]. Thus, for voltage systems using switches $\geq$3.3 kV, Type I switch is the preferred solution.

The maximum switching frequency at which the inverter is allowed to operate is dictated by the maximum allowable junction temperature of the device. The allowable junction temperature of the switch is set to be 90% of the absolute maximum junction temperature of the SiC MOSFET and Schottky diode. The SiC MOSFET and Schottky diode has a maximum junction temperature of 175°C, so the junction temperature of the devices in the CSI application is set to be 150°C. The average junction temperature of the semiconductors is calculated using (1).

$$T_j = T_{HS} + R_{jc} * P_{loss} \tag{1}$$

where T_j is the junction temperature of the DUT, R_{jc} is the junction to case thermal impedance obtained from the data sheet of the DUT, P_{loss} is the total switch loss (conduction and switching loss) of the DUT. T_{HS} is the heat sink temperature and is calculated using (2)

$$T_{HS} = T_{amb} + (R_{c,HS} + R_{HS,amb}) * P_{loss} \tag{2}$$

where T_{amb} is the ambient temperature, $R_{c,HS}$ is the case to heat sink temperature dictated by the thermal interface material (TIM), and $R_{HS,amb}$ is the thermal impedance of heat sink to ambient temperature thermal impedance obtained from the data sheet of the selected heat sink.

For a CSI, the current switch consists of the MOSFET and the diode, and it is necessary to observe both devices' maximum junction temperatures. The CSI is designed with an individual heat sink for each of the phases [34]. The TIM used for the device has a breakdown voltage of 5000 VAC. LAM6K 150 ME from Fischer Elektronik is the heat sink used for the CSI application. The ambient temperature is assumed to be 50°C. The average junction temperature of the SiC MOSFET and SiC Schottky diode is obtained at the rated dc-link current of 50 A at a variable switching frequency. Since the MOSFET losses comprise switching and conduction loss, the increased switching frequency increases the junction temperature of the MOSFET, as shown in Fig. 20a. However, the junction temperature of the diode is limited by the conduction loss dictated by the dc-link current. The maximum switching frequency of the 3.3 kV CSI is based on system parameters in Table. 2 operating at 50°C ambient is found to be 60 kHz. The inverter switching frequency is set to be 20 kHz as the dc-link inductor was designed to operate for a switching frequency ripple of 20 kHz. The junction temperature of the SiC MOSFET and SiC Schottky diode in a CSI operating at 20 kHz switching frequency and variable

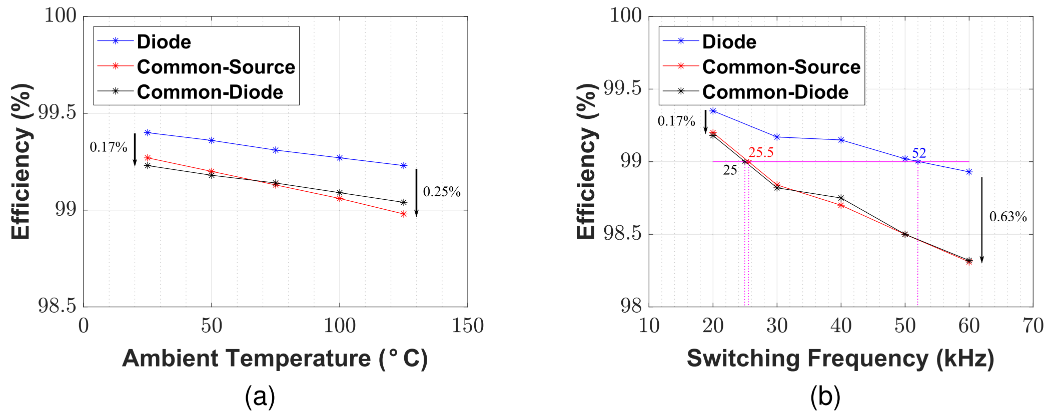

FIGURE 19. Efficiency of the CSI with three different switch configurations a) at various ambient temperatures, and b) at various switching frequencies.

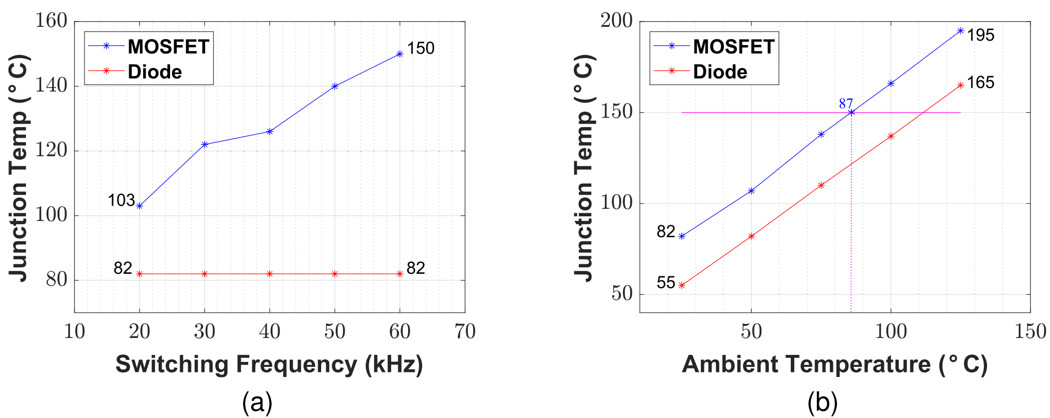

FIGURE 20. a) Junction temperature of the SiC MOSFET and SiC Schottky diode at various switching frequencies at an ambient temperature of 50°C, and b) Junction temperature of the SiC MOSFET and SiC Schottky diode at various ambient temperatures and switching frequency of 20 kHz.

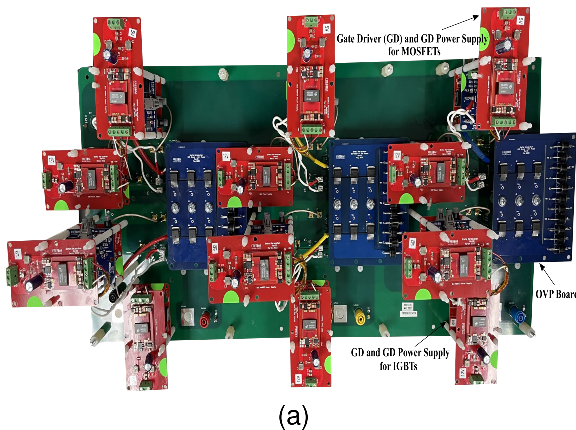

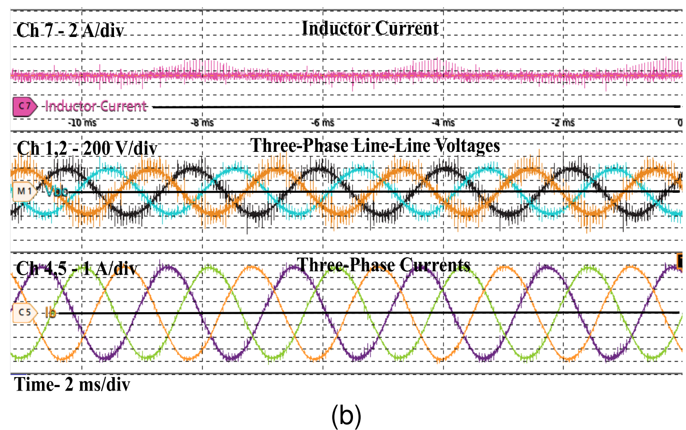

FIGURE 21. Experimental a) hardware prototype of a 3.3 kV Type I CSI, and b) normal operating mode results of a 3-ϕ CSI with an R-L load.

ambient temperatures is shown in Fig. 20b. The maximum permissible ambient temperature at which the switches can operate is 87°C.

The hardware prototype of the three-phase CSI with the 3.3 kV SiC MOSFET and Schottky diode is shown in Fig. 21a. The sinusoidal voltages and currents for the CSI are observed in Fig. 21b with the dc-link current of 5 A and the line-line voltage of 280 $V_{ll,rms}$ operating at room temperature, switching frequency of 20 kHz, and a fundamental frequency of 500 Hz. The input current source of the inverter is generated using a buck converter which is peak current controlled. The sinusoidal voltages and current make CSI a promising solution for motor drive applications.

V. CONCLUSION

This paper compares three SiC reverse voltage blocking switch types for an MV-based CSI application. The static characterization of the SiC MOSFET and SiC Schottky diode in TO-247 packages is discussed, which helps obtain the conduction losses of the CSI system. Also, the dynamic characterization of three switch configurations is evaluated for bidirectional voltage blocking capability and helps compute the switching losses. The turn-on and turn-off losses trend for the three-different switch configurations is discussed. The dependence of voltage and current on the switch type selection for a CSI application is presented. Based on the three-phase inverter system loss, the Type I-based switch with a MOSFET and a series diode is selected for the MV-based CSI for motor drive applications with 3.3 kV devices and higher voltage systems at a wide range of real-world operating points. The safe operating area of the Type I-based switch is then presented. Experimental results with the 3.3 kV Type I system operating with an R-L load show the superior performance of CSI with sinusoidal voltages and currents.

ACKNOWLEDGMENT

An earlier version of this paper was presented in part at the Conference Proceedings of WIPDA 2021 titled ''Performance Evaluation of 3.3 kV SiC MOSFET and Schottky Diode for Medium Voltage Current Source Inverter Application'' [DOI: 10.1109/WiPDA49284.2021.9645089].

REFERENCES

[1] A. Marzoughi, J. Wang, R. Burgos, and D. Boroyevich, ''Characterization and evaluation of the state-of-the-art 3.3-kV 400-A SiC MOSFETs,'' *IEEE Trans. Ind. Electron.*, vol. 64, no. 10, pp. 8247–8257, Oct. 2017.

[2] S. Narasimhan, S. Tewari, E. Severson, R. Baranwal, and N. Mohan, ''Mitigation of common-mode noise in wide band gap device based motor drives,'' in *Proc. IEEE Appl. Power Electron. Conf. Expo. (APEC)*, Mar. 2016, pp. 2043–2050.

[3] K. Hamada, S. Hino, N. Miura, H. Watanabe, S. Nakata, E. Suekawa, Y. Ebiike, M. Imaizumi, I. Umezaki, and S. Yamakawa, ''3.3 kV/1500 a power modules for the world's first all-sic traction inverter,'' *Jpn. J. Appl. Phys.*, vol. 54, Feb. 2015, Art. no. 04DP07.

[4] J.-I. Nakashima, A. Fukumoto, Y. Obiraki, Y. Mitsui, H. Nakatake, Y. Toyoda, A. Nishizawa, K. Kawahara, S. Hino, H. Watanabe, T. Negishi, and S.-I. Iura, ''6.5-kV full-SiC power module (HV100) with SBD-embedded SiC-MOSFETs,'' in *Proc. Conf. Power Electron., Intell. Motion, Renew. Energy Energy Manag.*, Jun. 2018, pp. 1–7.

[5] A. Anurag, S. Acharya, S. Bhattacharya, and T. R. Weatherford, ''Application of Gen-3 10 kV SiC MOSFETs in XHV-6 packaging for a mobile utility support equipment based solid state transformer (MUSE-SST),'' in *Proc. IECON 46th Annu. Conf. IEEE Ind. Electron. Soc.*, Oct. 2020, pp. 1291–1296.

[6] B. Wu and M. Narimani, *PWM Current Source Inverters*. Hoboken, NJ, USA: Wiley, 2017, pp. 225–256.

[7] F. Akbar and H. Cha, ''A novel three-phase H7 current-source inverter with improved reliability,'' in *Proc. IEEE Energy Convers. Congr. Expo. (ECCE)*, Sep. 2019, pp. 2836–2841.

[8] M. U. Hassan, A. I. Emon, F. Luo, and V. Solovyov, ''Design and validation of a 20-kVA, fully cryogenic, two-level GaN-based current source inverter for full electric aircrafts,'' *IEEE Trans. Transport. Electrific.*, vol. 8, no. 4, pp. 4743–4759, Dec. 2022.

[9] S. Narasimhan, A. Anurag, and S. Bhattacharya, ''Comparative study of a 3.3 kV SiC-based voltage and current source inverter for high-speed motor drive applications,'' in *Proc. IEEE 12th Energy Convers. Congr. Expo.*, May 2021, pp. 2211–2217.

[10] V. Madonna, G. Migliazza, P. Giangrande, E. Lorenzani, G. Buticchi, and M. Galea, ''The rebirth of the current source inverter: Advantages for aerospace motor design,'' *IEEE Ind. Electron. Mag.*, vol. 13, no. 4, pp. 65–76, Dec. 2019.

[11] H. Dai, R. A. Torres, T. M. Jahns, and B. Sarlioglu, ''Characterization and implementation of hybrid reverse-voltage-blocking and bidirectional switches using WBG devices in emerging motor drive applications,'' in *Proc. IEEE Appl. Power Electron. Conf. Expo.*, Mar. 2019, pp. 297–304.

[12] X. Han, L. Zheng, R. P. Kandula, K. Kandasamy, D. Divan, and M. Saeedifard, ''Characterization of 3.3-kV reverse-blocking SiC modules for use in current-source zero-voltage-switching converters,'' *IEEE Trans. Power Electron.*, vol. 36, no. 1, pp. 876–887, Jan. 2021.

[13] A. Kumar, S. Bhattacharya, J. Baliga, and V. Veliadis, ''Performance evaluation of 10 kV SiC current switch based PWM current source inverter for 4.16 kV motor drive applications,'' in *Proc. IEEE Appl. Power Electron. Conf. Expo. (APEC)*, Jun. 2021, pp. 1219–1226.

[14] N. R. Zargari, S. C. Rizzo, Y. Xiao, H. Iwamoto, K. Satoh, and J. F. Donlon, ''A new current-source converter using a symmetric gate-commutated thyristor (SGCT),'' *IEEE Trans. Ind. Appl.*, vol. 37, no. 3, pp. 896–903, 2001.

[15] Keysight Technologies. *B1505a Power Device Analyzer/Curve Tracer*. Accessed: Mar. 28, 2023. [Online]. Available: https://www.keysight.com/us/en/assets/7018-02115/data-sheets/5990-3853.pdf

[16] S. C. Rizzo, B. Wu, and R. Sotudeh, ''Symmetric GTO and snubber component characterization in PWM current-source inverters,'' *IEEE Trans. Power Electron.*, vol. 13, no. 4, pp. 617–625, Jul. 1998.

[17] K. Satoh, M. Yamamoto, K. Morishita, Y. Yamaguchi, and H. Iwamoto, ''High power symmetrical GCT for current source inverter,'' in *Proc. IEEE Int. Conf. Power Electron. Drive Syst.*, Jul. 1999, pp. 877–882.

[18] A. De, A. J. Morgan, V. M. Iyer, H. Ke, X. Zhao, K. Vechalapu, S. Bhattacharya, and D. C. Hopkins, ''Design, package, and hardware verification of a high-voltage current switch,'' *IEEE J. Emerg. Sel. Topics Power Electron.*, vol. 6, no. 1, pp. 441–450, Mar. 2018.

[19] A. De, S. Roy, and S. Bhattacharya, ''Comparative suitability evaluation of reverse-blocking IGBTs for current-source based converter,'' in *Proc. Int. Power Electron. Conf.*, May 2014, pp. 2562–2568.

[20] B. Jayant Baliga, *Fundamentals of Power Semiconductor Devices*. Berlin, Germany: Springer, 2008.

[21] C. DiMarino, Z. Chen, M. Danilovic, D. Boroyevich, R. Burgos, and P. Mattavelli, ''High-temperature characterization and comparison of 1.2 kV SiC power MOSFETs,'' in *Proc. IEEE Energy Convers. Congr. Expo.*, Sep. 2013, pp. 3235–3242.

[22] A. Kanale, B. J. Baliga, K. J. Han, and S. Bhattacharya, ''Experimental study of high-temperature switching performance of 1.2 kV SiC JBSFET in comparison with 1.2 kV SiC MOSFET,'' in *Proc. Mater. Sci. Forum*, 2019, pp. 625–628.

[23] R. Narwal, S. Rawat, A. Kanale, T.-H. Cheng, A. Agarwal, S. Bhattacharya, B. J. Baliga, and D. C. Hopkins, ''Analysis and characterization of four-quadrant switches based commutation cell,'' in *Proc. IEEE Appl. Power Electron. Conf. Expo. (APEC)*, Mar. 2023, pp. 209–216.

[24] *IPC-2221A: Generic Standard on Printed Board Design*. Accessed: May 2003. [Online]. Available: https://www.ipc.org/TOC/IPC-2221A.pdf

[25] *IPC-2221B: Generic Standard on Printed Board Design*. Accessed: Nov. 2012. [Online]. Available: https://www.ipc.org/TOC/IPC-2221B.pdf

[26] A. Kanale, S. Narasimhan, T.-H. Cheng, A. Agarwal, S. S. Shah, B. J. Baliga, S. Bhattacharya, and D. C. Hopkins, ''Comparison of the capacitances and switching losses of 1.2 kV common-source and common-drain bidirectional switch topologies,'' in *Proc. IEEE 8th Workshop Wide Bandgap Power Devices Appl. (WiPDA)*, Nov. 2021, pp. 112–117.

[27] K. Han, A. Agarwal, A. Kanale, B. J. Baliga, S. Bhattacharya, T.-H. Cheng, D. Hopkins, V. Amarasinghe, and J. Ransom, ''Monolithic 4-terminal 1.2 kV/20 a 4H-SiC bi-directional field effect transistor (BiDFET) with integrated JBS diodes,'' in *Proc. 32nd Int. Symp. Power Semiconductor Devices ICs (ISPSD)*, Sep. 2020, pp. 242–245.

[28] S. S. Shah, R. Narwal, S. Bhattacharya, A. Kanale, T.-H. Cheng, U. Mehrotra, A. Agarwal, B. J. Baliga, and D. C. Hopkins, ''Optimized AC/DC dual active bridge converter using monolithic SiC bidirectional FET (BiDFET) for solar PV applications,'' in *Proc. IEEE Energy Convers. Congr. Expo. (ECCE)*, Oct. 2021, pp. 568–575.

[29] S. Narasimhan, C. Sisson, S. Leslie, K. Parmar, S. K. Rastogi, and S. Bhattacharya, "Design considerations of a 3.3 kV SiC-based reverse voltage blocking module for current source inverter application," in *Proc. IEEE Appl. Power Electron. Conf. Expo. (APEC)*, Mar. 2023, pp. 350–357.

[30] B. J. Baliga, "Third generation PRESiCE technology for manufacturing SiC power devices in a 6-inch commercial foundry," *IEEE J. Electron Devices Soc.*, vol. 8, pp. 1111–1117, 2020.

[31] S. Mori, M. Aketa, T. Sakaguchi, H. Asahara, T. Nakamura, and T. Kimoto, "Demonstration of 3 kV 4H-SiC reverse blocking MOSFET," in *Proc. 28th Int. Symp. Power Semiconductor Devices ICs (ISPSD)*, Jun. 2016, pp. 271–274.

[32] R. A. Torres, H. Dai, W. Lee, B. Sarlioglu, and T. Jahns, "Current-source inverter integrated motor drives using dual-gate four-quadrant wide-bandgap power switches," *IEEE Trans. Ind. Appl.*, vol. 57, no. 5, pp. 5183–5198, Sep. 2021.

[33] R. A. Torres, H. Dai, T. M. Jahns, and B. Sarlioglu, "Operation and analysis of current-source inverters using dual-gate four-quadrant wide-bandgap power switches," in *Proc. IEEE Energy Convers. Congr. Expo. (ECCE)*, Sep. 2019, pp. 2353–2360.

[34] A. Thermalloy, "Interface materials—Electrically isolating—Pads," Aavid Thermalloy, Laconia, NH, USA, Tech. Rep. [Online]. Available: https://www.mouser.com/catalog/specsheets/Aavid_11192018_524e1b33e825a55cbb0e6acead33a15f.pdf

[35] S. Narasimhan, A. Kanale, S. Bhattacharya, and J. Baliga, "Performance evaluation of 3.3 kV SiC MOSFET and Schottky diode for medium voltage current source inverter application," in *Proc. IEEE 8th Workshop Wide Bandgap Power Devices Appl. (WiPDA)*, Nov. 2021, pp. 366–371.

SNEHA NARASIMHAN (Graduate Student Member, IEEE) received the B.Tech. degree in electrical and electronics engineering from Amrita University, India, in 2013, and the M.S. degree in electrical engineering from the University of Minnesota, in 2015. She is currently pursuing the Ph.D. degree with the FREEDM Systems Center, North Carolina State University, Raleigh, NC, USA.

Prior to joining the Ph.D., she was with Rockwell Automation, as an Associate Hardware Engineer. During the Ph.D. study, she has interned with the ABB Corporate Research Center, Raleigh. Her current research interests include wide band-gap devices, current source inverters, and high-speed motor drives.

Ms. Narasimhan was recognized as a Graduate Student of the Year for Scholarly Achievement with NC State, in 2023. She is currently the IEEE Power Electronics Society (PELS) Women in Engineering (WiE) Treasurer.

AJIT KANALE (Member, IEEE) received the B.Tech. degree in avionics from the Indian Institute of Space Science and Technology, Thiruvananthapuram, India, in 2012, and the M.S. and Ph.D. degrees in electrical engineering from North Carolina State University, Raleigh, NC, USA, in 2019 and 2022, respectively.

Currently, he is a Power Applications Engineer with Wolfspeed Inc. His research interests include power semiconductor device characterization, failure and reliability analysis, and the design of gate drivers and power converters.

SUBHASHISH BHATTACHARYA (Fellow, IEEE) received the B.E. degree from IIT Roorkee, Roorkee, India, the M.E. degree from the Indian Institute of Science, Bengaluru, India, and the Ph.D. degree from the University of Wisconsin-Madison, Madison, WI, USA, in 2003, all in electrical engineering.

He was with the Flexible AC Transmission Systems (FACTS) and Power Quality Group, Westinghouse Research and Development Center, Pittsburgh, which later became part of Siemens Power Transmission and Distribution, from 1998 to 2005. He joined the Department of Electrical and Computer Engineering, North Carolina State University (NCSU), in August 2005, where he is the Duke Energy Distinguished Professor and a Founding Faculty Member of the NSF ERC FREEDM Systems Center, the Advanced Transportation Energy Center (ATEC), the U.S. DOE Initiative on WBG Based Manufacturing Innovation Institute, the PowerAmerica, NCSU. A part of his Ph.D. research on active power filters was commercialized by York Corporation Inc. (currently part of Johnson Controls) for air-conditioner chiller products. His research was funded by several industries, such as NSF, DOE, ARPA-E, U.S. Navy, ONR, and NASA. He has over 500 publications and ten patents and several pending patent applications. His research interests include solid-state transformers, integration of renewable energy resources, MV power converters enabled by HV SiC devices, FACTS, utility applications of power electronics and power quality issues, dc microgrids, high-frequency magnetics, active filters, and application of new power semiconductor devices, such as SiC and GaN for converter topologies.

JAYANT B. BALIGA (Life Fellow, IEEE) received the M.S. and Ph.D. degrees in electrical engineering from the Rensselaer Polytechnic Institute, Troy, NY, USA, in 1971 and 1974, respectively.

He is internationally recognized for his leadership in the area of power semiconductor devices. He has authored and edited over 22 books, 650 publications in international journals and conference digests, and received over 121 U.S. patents. In 2016, he was inducted into the National Inventors Hall of Fame as the Sole Inventor of IGBT. He received the National Medal of Technology and Innovation from President Obama, in 2011; the North Carolina Award for Science from Governor Purdue, in 2012; the IEEE Medal of Honor, in 2014; and the 2015 Global Energy Prize in St. Petersburg, Russia.